Lewis Acid Pairs for the Activation of Biomass-derived Oxygenates in Aqueous Media

DOE Grant: DE-SC0008742
PI: Román, Yuriy
Graduate students: Luo, Helen and Lewis, Jennifer D.
Affiliations: Department of Chemical Engineering, Massachusetts Institute of Technology
Contact: 77 Massachusetts Ave 66-456, Cambridge MA, 20139 Ph: 617-253-7090
Yearly Budget: $450,000
Period of Execution: 09/15/2012 – 09/14/2015
Year grant started: 2012

A) Abstract

The objective of this project is to understand the mechanistic aspects behind the cooperative activation of oxygenates by catalytic pairs in aqueous media. Specifically, we will investigate how the reactivity of a solid Lewis acid can be modulated by pairing the active site with other catalytic sites at the molecular level, with the ultimate goal of enhancing activation of targeted functional groups. Although unusual catalytic properties have been attributed to the cooperative effects promoted by such catalytic pairs, virtually no studies exist detailing the use heterogeneous water-tolerant Lewis pairs. A main goal of this work is to devise rational pathways for the synthesis of porous heterogeneous catalysts featuring isolated Lewis pairs that are active in the transformation of biomass-derived oxygenates in the presence of bulk water. Achieving this technical goal will require closely linking advanced synthesis techniques; detailed kinetic and mechanistic investigations; strict thermodynamic arguments; and comprehensive characterization studies of both materials and reaction intermediates.

For the last performance period (2014-2015), two technical aims were pursued:

1) C-C coupling using Lewis acid and base pairs in Lewis acidic zeolites. Tin-, zirconium-, and hafnium containing zeolites (e.g., Sn-, Zr-, and Hf-Beta) are versatile solid Lewis acids that selectively activate carbonyl functional groups. In this aim, we demonstrate that these zeolites catalyze the cross-aldol condensation of aromatic aldehydes with acetone under mild reaction conditions with near quantitative yields. NMR studies with isotopically labeled molecules confirm that acid-base pairs in the Si-O-M framework ensemble promote soft enolization through α-proton abstraction. The Lewis acidic zeolites maintain activity in the presence of water and, unlike traditional base catalysts, in acidic solutions.

2) One-pot synthesis of MWW zeolite nanosheets for activation of bulky substrates. Through post-synthetic modifications, layered zeolite precursors can be transformed into 2-dimensional (2D), zeolites with open architectures. These novel hierarchical microporous/mesoporous materials with exposed active sites can facilitate the

conversion of bulky substrates while maintaining higher stability than amorphous mesoporous materials. However, post-synthetic exfoliation techniques are energy intensive, multi-step and require highly alkaline conditions that result in low silica yields and a partially amorphous product. In this aim, we demonstrate an effective one-pot synthesis method to generate exfoliated single-unit-cell thick MWW nanosheets. The new material, named MIT-1, is synthesized using a rationally-designed OSDA and results in a material with high crystallinity, surface area, and acidity that does not require post-synthetic treatments other than calcination. A parametric study of Al, Na, and water content reveals that MIT-1 crystallizes over a wide synthetic window. Characterization data show that MIT-1 has high mesoporosity with an external surface area exceeding 500 m^2g^{-1} and a high external acid site density of 21 x 10^{-5} mol g^{-1}. Catalytic tests demonstrate that MIT-1 has three-fold higher catalytic activity for the Friedel-Crafts alkylation of benzene with benzyl alcohol as compared to that of other 3D MWW topology zeolites.

B) Results and discussion

Aim 1a: Investigation of carbonyl activation and α-proton extraction by Lewis acidic zeolites

Motivation and Objectives

Lewis acidic zeolites have recently emerged as exceptional catalysts for the activation of carbonyl-containing molecules, which makes them a potential catalyst for promoting C-C coupling between aldehydes and ketones. Akin to hybrid organic-inorganic aminosilica materials [1] and enzymatic systems,[2, 3] the acid-base pairs in these inorganic solids are capable of cooperatively activating carbonyl compounds. While Sn-Beta has recently been shown to promote the self-aldol addition of glycolaldehyde [4] and the aldol condensation of 1,3-dihydroxyacetone with glyceraldehyde [5] and formaldehyde,[6] C-C coupling with Lewis acidic zeolites is still poorly understood. According to our proposed mechanism shown in Scheme 1, the metal center polarizes the carbonyl group of acetone, which acidifies the α-proton. The framework oxygen atom bound to the metal atom acts as a base that abstracts the α-proton, thereby generating a silanol group and a metal enolate that readily undergoes C-C coupling with aldehydes. We utilized isotopic labeling studies to show that framework acid-base pairs promote keto-enol tautomerization through the transfer of an α-proton to the zeolite lattice.

Scheme 1. Proposed reaction mechanism for the aldol condensation of benzaldehyde (BA) and acetone catalyzed by Lewis acidic Beta zeolites. M=metal atom; X^1=the zeolite framework beginning with OSi_3; and X^2=OSi_3 or OH.

Approach

Fully deuterated acetone ([D_6]acetone) was used for ^{13}C and ^{1}H NMR spectroscopic studies on the reversible keto-enol tautomerization of acetone in the presence of either Hf-Beta or Sn-Beta. As shown in Scheme 2, a mechanism proceeding via a metal enolate using [D_6]acetone would result in the transfer of an α-deuterium to form a silanol group in the zeolite framework. This deuterium atom would readily scramble in the presence of unlabeled hydroxy groups.

Scheme 2. Mechanistic pathway of acetone enolate formation at Hf- and Sn-Beta active sites.

Solutions for the enolate study were prepared with 5 wt% [D6]acetone in tert-butanol (tButOH) and [D6]benzene such that the molar ratio of [D6]acetone to tButOH was 1:6. Solutions with reversed isotopic labeling used acetone instead of [D6]acetone and tButOD instead of tButOH. Hf-Beta was added such that (mmol [D6]acetone)/(mmol Hf) = 100:1. Reaction mixtures were sealed in 5 mL glass reactors and heated to 363 K for 4 or 8 h. Solids were removed by a 0.2 mm Millipore PTFE syringe filter before analysis by GC–MS and NMR.

Results

The ^{13}C NMR spectra in Figure 1 show that upon heating to 363 K for 8 hours in the presence of Hf-Beta and *t*BuOH, [D_6]acetone progressively lost its isotopic labels. Prior to reaction, the spectrum of [D_6]acetone displayed the expected 1:3:6:7:6:3:1 septet for the methyl carbon atoms. After the reaction, a 1:2:3:2:1 quintet, a 1:1:1 triplet, and a singlet were observed, which correspond to acetone molecules with CD_2H, CDH_2, and CH_3 groups, respectively. These signals exhibit the characteristic

splitting pattern resulting from ^{13}C-^{2}H J coupling and are shifted by -0.25 ppm, from δ=29.58 ppm, per proton added from [D_6]acetone because of the isotope effect. Deuteron-proton exchange is also supported by the observed changes in the ^{13}C NMR resonances of the carbonyl carbon atom and ^{1}H NMR signals that are consistent with methyl groups on partially deuterated acetone, as well as a decrease in the molecular weight of acetone as confirmed by mass spectrometry. Identical results were observed with Sn-Beta. Acetone condensation products were not detected with either catalyst. Experiments conducted with reversed isotopic labeling (i.e., using acetone and [D]tert-butanol) showed the expected ^{13}C NMR resonance changes and larger mass fragments in the mass spectrum. Importantly, control reactions with Si-Beta and without catalyst did not change the chemical environment of [D_6]acetone. We note that diffuse reflectance UV-visible (DRUV) and ^{119}Sn NMR spectra (for Sn-Beta) rule out the presence of high concentrations of extra-framework species. Taken together, these data clearly show that framework sites in Lewis acidic zeolites enolize acetone by activating its α-hydrogen atoms. Similarly, Bell et al. showed that oxygen atoms with increased basicity in the first coordination sphere of the active site in Sn-Beta abstract protons from hydroxy groups of glucose to facilitate ring-opening for isomerization reactions.[7] Our results are also intriguing in view of the studies by Davis et al. showing that framework sites catalyze the isomerization of glucose into fructose in water through an intramolecular CH hydride shift, whereas extra-framework SnO_2 sites catalyze the reactions by proton transfer and enolization.[8] Evidently, enolization with framework sites is dependent on the nature of the metal center, the substrate, and the solvent.

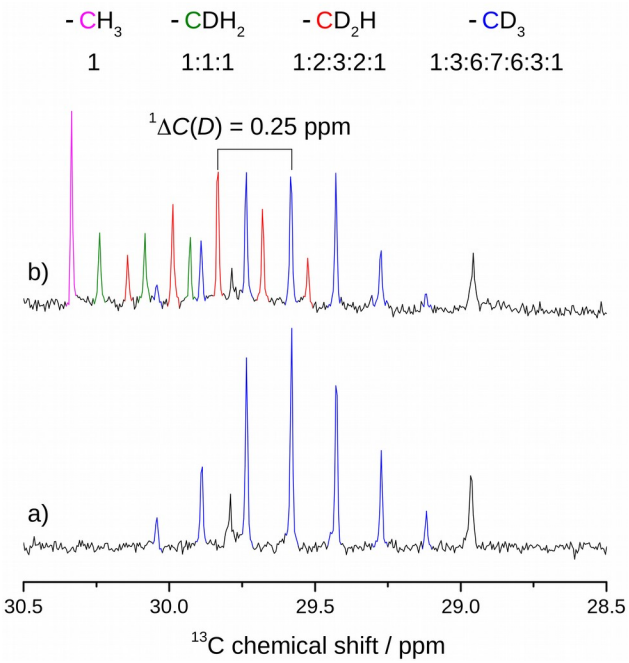

Figure 1. ^{13}C NMR spectra of [D_6]acetone before (a) and after (b) reaction in the presence of Hf-Beta and *t*BuOH at 363 K for 8 h.

Future Work

To further understand the reaction mechanism, we plan to focus on understanding the role of closed and open sites for aldol condensation. We will use probe molecules in conjunction with solid state NMR to more fully characterize the molecular connectivity at the active site.

Aim 1b: Investigation of the catalytic activity of Lewis acidic Beta zeolites for C-C coupling

Motivation and Objectives

Aldol condensation is a key carbon-carbon coupling reaction in organic synthesis and has triggered considerable interest in the development of biomass conversion schemes. For example, the cross-aldol reaction between furfural derivatives and acetone has been exploited to generate C_8-C_{15} hydrocarbons using metal oxides,[9] hydrotalcites,[10] and homogeneous mineral base catalysts.[11] Strong bases are typically used because they readily abstract α-protons and generate the enolate intermediate required for C-C bond formation. However, the use of base catalysts for these reactions faces major challenges. Homogeneous mineral bases are unable to activate molecules with hydroxycarbonyl groups because of the preferential formation of alkoxide ions, and they require more complex separations. Solid bases are preferable, but they easily deactivate in the presence of acids, such as acetic acid, which are ubiquitous in biomass processing. Lewis acidic zeolites have recently emerged as exceptional catalysts for the activation of carbonyl-containing molecules, thus affording the opportunity to promote aldol reactions under conditions that are generally considered unsuitable for direct C-C bond formation. In this aim, we show that Hf-, Sn-, and Zr-Beta zeolites are highly active catalysts for the cross-aldol condensation of aromatic aldehydes with acetone under mild reaction conditions. We also demonstrate how Lewis acidic zeolites can tolerate common poisons and regeneration by thermal treatments.

Approach

The aldol condensation of benzaldehyde (BA) with acetone in toluene was used as a model reaction to study the catalytic performance of a range of Lewis acidic zeolites in batch reactions. Catalysts tested included the Lewis acidic zeolites Hf-, Sn-, Zr-, and Ti-Beta, along with controls of HfO_2 impregnated Si-Beta, Si-Beta, Al-Beta, and no catalyst. The three most active catalysts, Hf-, Sn-, and Zr-Beta were also tested for the aldol condensation of acetone with a range of aromatic aldehydes including 4-substituted benzaldehydes and 5-(hydroxymethyl)furfural (HMF). Catalyst stability was probed using recyclability tests. Tolerence to common biomass-system poisons was evaluated by adding acetic acid and water to the reaction solution.

Results

The catalytic results for the aldol condensation of benzaldehyde and acetone promoted by Lewis acidic zeolites are shown in Table 1. Hf- and Zr-Beta showed the highest aldol condensation activity at 363 K, achieving conversions of more than 90 % with up to 97 % selectivity toward the dehydrated cross-aldol product, benzalacetone (2). The fact that the hydrated product, 4-hydroxy-4-phenyl-2-butanone (1), could not be detected indicates that the

dehydration reaction is fast under these reaction conditions. The double cross-aldol condensation product dibenzalacetone (3) was not produced either, which is likely attributable to steric hindrance caused by the zeolite pore. Ti-Beta yielded negligible aldol condensation products. Control reactions with Al-Beta, Si-Beta, extra-framework HfO_2 nanoparticles impregnated on Si-Beta (HfO_2/Si-Beta), and reactions without the catalyst confirmed that framework Lewis acidic heteroatoms are required for catalytic activity.

The observed difference between the various Beta zeolites is consistent with previous studies, which indicated that catalytic activity is dependent on the polarizability of the metal atom in the active site and the Brønsted basicity of the associated oxygen atom.[7] The d-block transition metals Hf and Zr possess similar electronic structures when inserted in the zeolite framework and can be expected to show similar catalytic activity, while the p-block element Sn exhibits different bonding characteristics and charge distribution through the site because of its antibonding σ* LUMO.[7, 12] We next extended our study to include several BA derivatives (Table 1, entries 2-4). The observed trend in catalytic activity of the metal centers is similar to the one seen for reactions with BA: Hf≈Zr>Sn. Selectivity toward the desired single cross-aldol condensation product remained over 90 % when using Hf- and Zr-Beta. Sn-Beta, in contrast, only reached 86 and 78 % selectivity when starting from 4-nitrobenzaldehyde and 4-chlorobenzaldehyde, respectively. A comparison between BA derivatives shows a decrease in activity with the addition of both electron-withdrawing and electron-donating groups, a trend not solely characteristic of strong base or acid catalysts. This mixed trend is indicative of a cooperative effect between weak acid and base sites in the zeolite. Additionally, steric limitations in the pores of zeolite Beta may impede transition-state formation for benzaldehyde analogues with larger substituents at the 4-position. The aldol reaction between HMF and acetone was also examined (Table 1, entry 5), as this is a potential pathway to produce liquid alkanes from biomass.[9] Reactions with both Hf- and Zr-Beta generated the single cross-aldol product with selectivities of 99 and 87 %, respectively, at similar conversions. Surprisingly, reactions catalyzed by Sn-Beta only generated undesired polymerization products.

Table 1. Experimental results of the cross-aldol condensation of aldehydes with acetone using Lewis acid zeolites.[a]

Entry	Aldehyde	Catalyst	Conversion [%] [b]	Selectivity [%] [c]
1		Hf-Beta	91	97
		Sn-Beta	32	90
		Zr-Beta	94	98
2		Hf-Beta	38	96
		Sn-Beta	28	86
		Zr-Beta	48	97
3		Hf-Beta	69	90
		Sn-Beta	25	78
		Zr-Beta	78	90
4		Hf-Beta	27	98
		Sn-Beta	19	96
		Zr-Beta	42	>99
5		Hf-Beta	73	>99

	Sn-Beta	32	0
	Zr-Beta	72	87

[a] Reaction conditions: 0.084 M aldehyde in toluene, (mmol acetone):(mmol aldehyde):(mmol metal) = 150:50:1, 363 K, 5 h. [b] Conversion: [mmol(aldehyde converted)]/[mmol(aldehyde initial)] × 100. [c] Selectivity: [mmol(single cross-aldol condensation product)]/[mmol(aldehyde converted)] ×100.

The stability of Hf-Beta for the aldol condensation of BA and acetone was probed by reusing the catalyst with fresh solution for five consecutive batch reactions (see Figure 2). Conversion decreased by 18^% between the first and second runs, and it remained constant for subsequent runs. In all cases, selectivity for **2** remained above 98 %. Calcination between the fourth and fifth runs did not alter activity. Thermogravimetric analysis showed a 2 % weight loss, which we ascribe to the presence of organic components within the zeolite pores after reaction. These results are consistent with the observed deactivation behavior of Hf-Beta during catalytic transfer hydrogenation reactions.[13] Hot filtration tests confirmed the heterogeneous nature of the catalytic system.

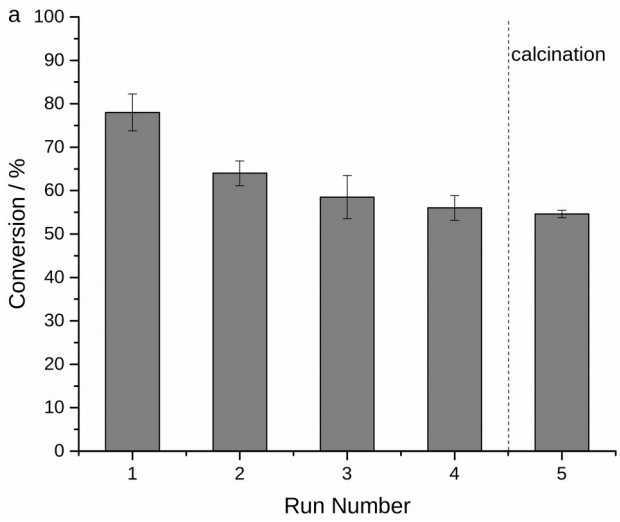

Figure 2. Conversion for recycle runs for Hf-Beta in the aldol condensation of BA with acetone. Reactions were run for 2 h before separating the catalyst by centrifugation and decantation. Fresh solution was added for each subsequent run. The catalyst was washed with acetone and calcined at 853 K in flowing air between runs 4 and 5. The five cycle test was equivalent to ca. 150 turnovers per Hf site.

Organic acid impurities can deactivate strong base catalysts, while water may react undesirably with homogeneous Lewis acids. Thus, Hf-Beta was tested in the presence of these components for the aldol condensation of BA and acetone (Figure 3). Unlike traditional base catalysts, Hf-Beta was not quenched by the presence of acetic acid. Although conversion decreased by 35 % upon adding 0.11 wt % acetic acid (i.e., a molar ratio of 1:5 acetic acid/BA), the zeolite generated the desired product with a selectivity of 93 %. Conversely, the solid base catalyst MgO showed almost no activity in the presence of acetic acid. Furthermore, MgO only achieved 42 % selectivity for **2** under acid-free conditions, primarily because of the production of **3**. Figure 3b shows that Hf-Beta is capable of catalyzing the aldol

condensation with as much as 10 wt% water, although conversions decreased by 50 % when compared to the dry reaction. Note that acetone was used as the solvent for the water tests because of the immiscibility of water with toluene. In pure acetone, reaction rates were lower compared to those obtained in toluene. We hypothesize that high acetone concentrations hinder BA adsorption because of competitive interaction with the Lewis acidic sites. Indeed, self-aldol reaction of acetone to form mesityl oxide and diacetone alcohol was observed in small quantities (<2 %). Reactions in acetone also displayed lower selectivity for **2** because of reduced dehydration of the aldol addition product **1**. As expected, the selectivity for **1** increased with higher water concentrations, as water is a by-product of aldol condensation. A reaction with both water and acetic acid impurities (Figure 3b, entry marked 1*) showed that Hf-Beta remains active even when multiple contaminants are present.

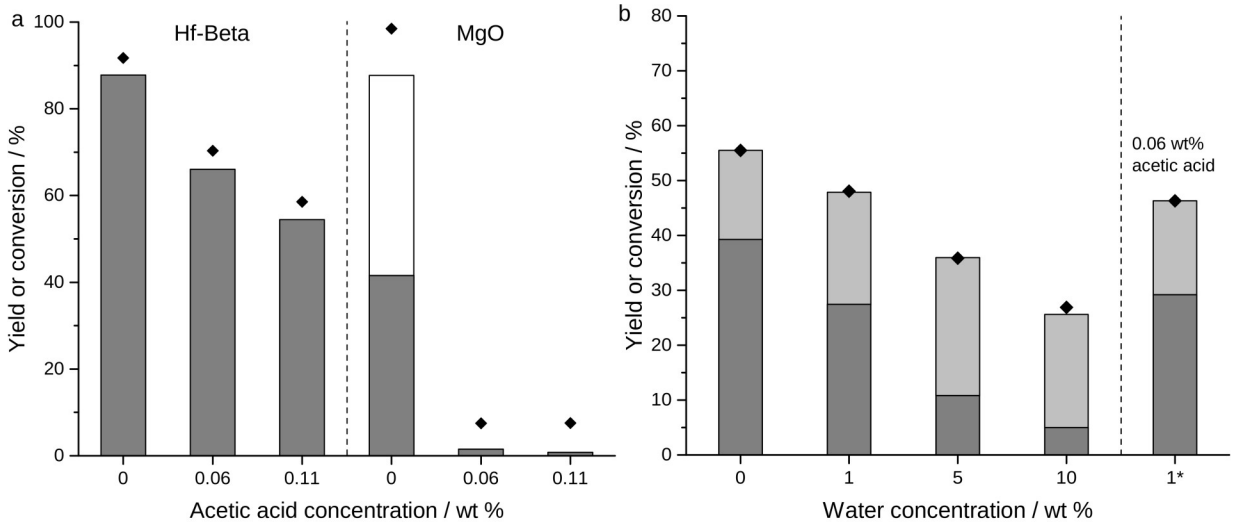

Figure 3. Effects of a) acetic acid and b) water on aldol condensation of BA and acetone. Reaction conditions: same as Table 1, MgO loaded at 2 wt% for (a), and acetone used as a solvent for (b). Acetic acid concentrations of 0.06 and 0.11 wt% correspond to molar ratios of acetic acid:BA:Hf = 5:50:1 and 10:50:1, respectively. Water concentrations of 1, 5, and 10 wt% correspond to molar ratios of water:BA:Hf = 300:50:1, 1500:50:1, and 3000:50:1, respectively. Entry 1* on (b) had both water and acetic acid impurities with molar ratios of water:acetic acid:BA:Hf = 300:5:50:1. Legend: Yields of ▒ **1**, ■ **2**, and □ **3**; ♦ Conversion.

Future Work

The long-term stability of Hf-Beta for these reactions will be probed using a packed bed reactor system. We also plan to expand our knowledge of C-C coupling with Lewis acidic zeolites by exploring other target reactions where carbonyl activation is key.

Aim 2a: Develop and optimize the one-pot synthesis of single-unit-cell thick MWW zeolite nanosheets

Motivation and Objectives

In recent years, layered zeolite precursors have garnered increased attention as a platform for developing new materials. An important aluminosilicate layered zeolite precursor is MCM-22(P)[14, 15], which forms in single unit-cell thick (ca. 2.5 nm) layers with the MWW topology. These layers are arranged perpendicular to the c-axis such that half of the 12-ring cage is exposed to the crystal exterior, effectively forming “cups” of fully connected tetrahedral atoms on each side of the layer (see Scheme 3).[16] In contrast to typical surface acid sites, the Brønsted acid sites located in the cups are as strong as those located inside micropores.[17, 18] Unfortunately, upon calcination, the layers of MCMC-22(P) condense topotactically to form the microporous three-dimensional (3D) zeolite MCM-22 (12-ring cages connected by 10-ring channels). As such, post-synthetic methods have been developed to prevent layer condensation and generate exfoliated MWW nanosheets with a large fraction of exposed cups. Corma et al. developed ITQ-2 by swelling the layers of MCM-22(P) with a quaternary ammonium surfactant and then delaminating the swollen sheets by ultrasonication.[19] The calcined material, comprised of disordered sheets, featured very high external surface areas of ca. 700 m^2g^{-1} and was shown to be active for the cracking of vacuum gas oil,[19] decalin and tetralin,[20] as well as the isomerization of m-xylene.[21] Exfoliation was shown to be most effective over a specific set of conditions that include using highly alkaline conditions (pH > 12.5 at 353 K)[21] and precursor materials with Si/Al ratios >20.[22] Although one-pot synthesis methods are preferable for process intensification, they have been largely unsuccessful in creating materials with comparable properties to those obtained with multi-step, post-synthetic methods. For example, zeolites MCM-56,[23-25] ITQ-30,[26] and EMM-10[27] exhibit a degree of disorder in the stacking of layers perpendicular to the c-axis, but their low mesoporosity indicates their structure more closely resembles their 3D counterparts. Consequently, the development of an effective and robust method to create high-quality MWW nanosheets without additional post-synthetic treatments continues to be challenging. Here, we demonstrate an effective one-pot synthesis method to generate exfoliated single-unit-cell thick MWW nanosheets.

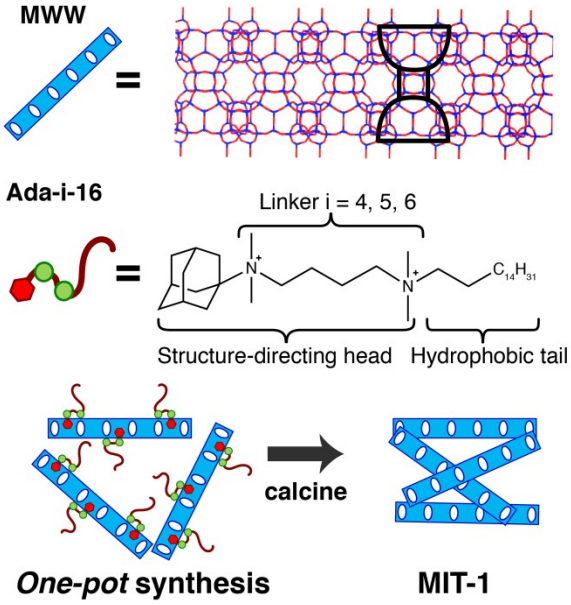

Scheme 3. Schematic representation of the one-pot synthesis strategy to create MIT-1.

Approach

The strategy to design an OSDA that could produce MWW nanosheets in one-pot is depicted in Scheme 3. We surmised that a suitable OSDA should combine the elements of the traditional OSDA used for the synthesis of layered zeolite precursor and the quaternary ammonium surfactant typically used for the swelling step during post-synthetic delamination. MCM-22(P) can be synthesized using hexamethyleneimine (HMI) or trimethyladamantylammonium hydroxide (Ada-OH), while swelling is typically performed with hexadecyltrimethylammonium bromide (CTAB). As shown in Scheme 3, the novel OSDA, named Ada-i-16 (where i = 4, 5, or 6 $–CH_2–$ linker groups), has a hydrophobic tail segment that resembles CTAB, a hydrophilic head segment that resembles Ada-OH, and a di-quaternary ammonium linker that connects both segments. The linker ammonium composition and chain length was tuned to achieve an effective C/N^+ ratio ranging from 17-18, which is close to the optimal (10-15) identified for high silica hydroxide syntheses,[28, 29] and which decreases the risk of solubility problems for the OSDA in water. We varied the linker size between 4 and 6 $–CH_2–$ units because the linker size can affect the mobility and interdigitation of the C_{16} tails, thereby influencing the packing (*i.e.*, unilamellar vs. multilamellar) of the layers.[30] Molecular dynamics simulations indicate that the structure-directing head sits inside of the cups with the diquaternary ammonium moieties stabilizing the pore mouth.

Results

An initial screening to understand the effect of Ada-i-16 composition on MIT-1 crystallization was investigated using a synthesis gel of 1 SiO_2/0.1 Ada-i-16 /0.05 $Al(OH)_3$/0.2 NaOH/45 H_2O at 433 K with rotation at 60 rpm. Varying the linker size drastically affected the crystallization time. Specifically, fully crystalline MIT-1 was obtained in 14 and 22 days when using Ada-4-16 and Ada-6-16, respectively. Interestingly, the C_5 linker did not yield a crystalline product even after 30 days. ^{13}C magic-angle spinning nuclear magnetic resonance (MAS NMR) on the as synthesized material confirms that the OSDA remains intact in the pores. Increasing the Ada-4-16/Si ratio up to 0.3 did not affect the synthesis time or phase purity. Decreasing the temperature from 433 K to 423 K doubled the synthesis time, but did not alter the product phase. A parametric study of Al, Na, and water content was conducted to determine the synthesis window for MIT-1. The synthesis space closely mirrors the space for phase-pure MCM-22(P). At Si/Al ratios below 12, only amorphous product is observed, while at Si/Al ratios above 70, competing MFI phases are observed. Materials synthesized in the absence of Al consistently resulted in a disordered MRE topology (ZSM-48).[31-33] Increasing the NaOH/Si from 0.2 to 0.3 decreased the crystallization time from 14 to 7 days. Decreasing the NaOH/Si to 0.1 increased the crystallization time to 30 days. This modulation of crystallization time likely arises from the increase in OH^- content, since substituting NaCl as a sodium source resulted in an amorphous product. Increasing the H_2O/Si ratio above 30 did not influence crystallization, but lower water contents generated only amorphous phases.

The powder X-ray diffraction patterns (PXRD) acquired after calcination of MIT-1 (synthesized with Ada-4-16) at 813 K for 10 h confirm that the sample has the MWW topology (Figure 4A). The diffraction pattern features broader peaks than those observed for MCM-22. More specifically, the pattern shows reflections belonging to the (*hk0*) directions, indicating the absence of long-range order in the c-direction, as expected for exfoliated MWW layers.[34] Simulated diffraction patterns (obtained using powder pattern theorem for ultrasmall zeolite crystals implemented with UDSKIP)[35, 36] for MWW crystalline constructs that are 15 unit cells wide along the *a*- and *b*-axes and one unit-cell thick along the c-axis are in good agreement with the experimental PXRD patterns for MIT-1. Scanning electron microscopy of MIT-1 reveal particles composed of disordered platelets agglomerated into >10 μm clusters (Figure 5). No other morphologies were detected during low magnification inspections. TEM confirmed the presence of disordered nanosheets ca. 2.5 nm thick along the (*001*) direction and ca. 150 nm (spanning 50-200 nm) long along the (*100*) and (*010*) directions. Selected area electron diffraction perpendicular to the plane of the sheets (inset, Figure 5) reveals the expected hexagonal symmetry of MWW topology crystals. Nitrogen adsorption studies demonstrate that MIT-1 has much higher mesoporosity than MCM-22 or MCM-56 with a very broad mesopore size distribution (see Figure 4C). The total pore volume and external surface area of MIT-1 after calcination are 1.014 cm^3g^{-1} and 513 m^2g^{-1}, respectively. This surface area is very close to the theoretical value of 517 m^2g^{-1} calculated for 150x150 nm long and 2.5 nm thick MWW sheets using geometric arguments. In contrast, the total pore volume and external surface area of MCM-22 are three times lower at 0.289 cm^3g^{-1} and 121 m^2g^{-1}, respectively. For MCM-56, the total pore volume and external surface area are two times lower at 0.601 cm^3g^{-1} and 219 m^2g^{-1}, respectively. A log-plot of the adsorption isotherms (Figure 4C, inset) shows that, in the pressure range of 10^{-7} to 10^{-3} P/P_0, MIT-1 has a lower N_2 uptake than MCM-22, which is consistent with the loss of the 10-ring channels associated with the 12-ring supercages along the *c*-axis.[37] Taken together, the characterization data confirm that MIT-1 is a highly crystalline delaminated MWW material with high surface area and mesoporosity.

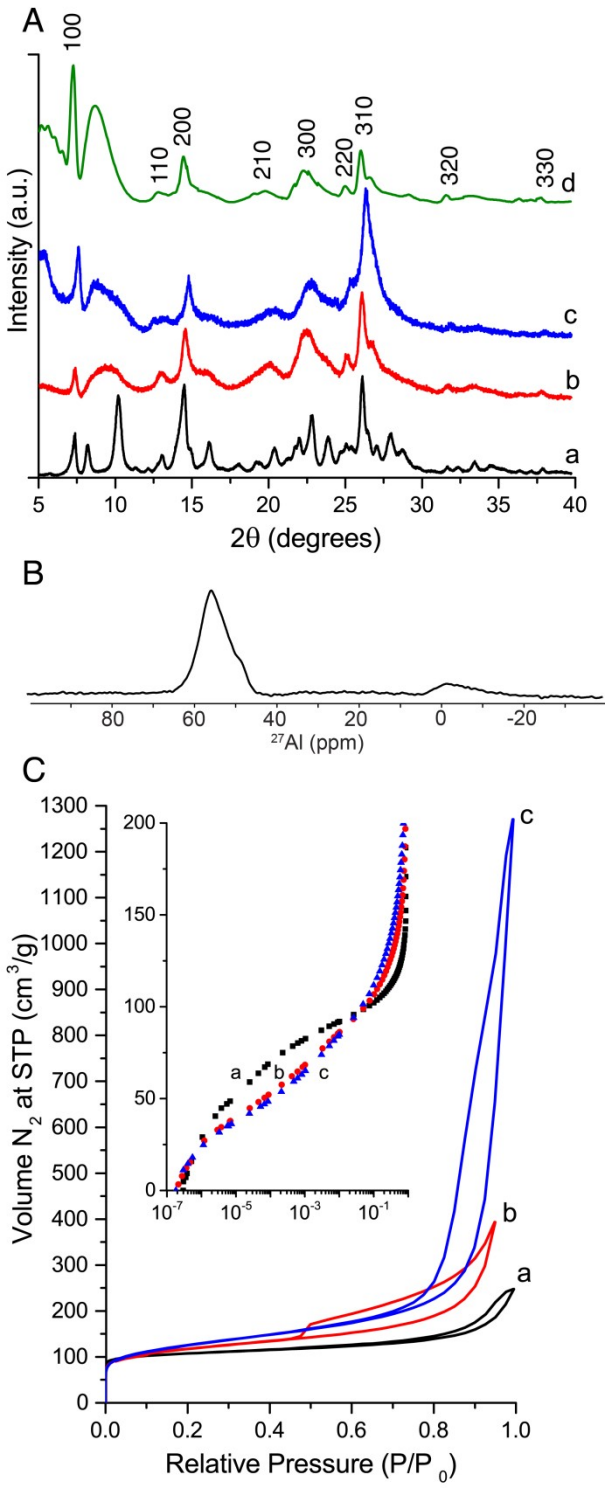

Figure 4. Powder XRD patterns (A) for calcined MCM-22 (a), MCM-56 (b), MIT-1 (c), simulated MWW nanosheets (d). ^{27}Al MAS NMR spectra of as-synthesized MIT-1 (B). N_2 adsorption and desorption isotherms (C) for calcined MCM-22 (a), MCM-56 (b), MIT-1 (c). Inset shows data on a semi-log plot.

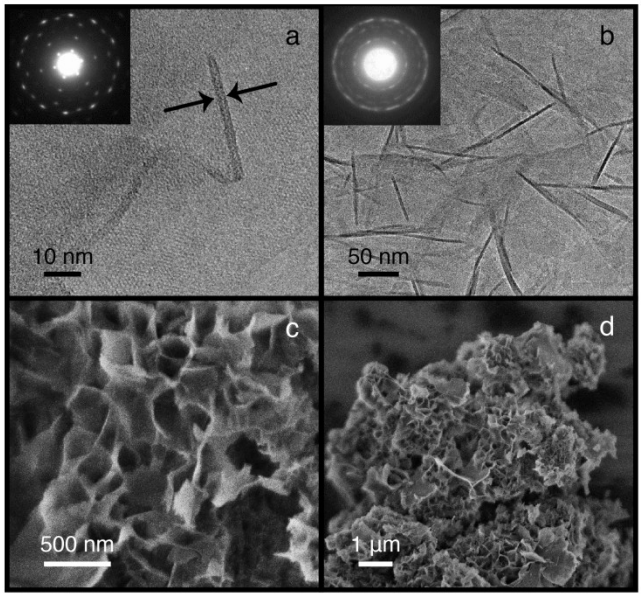

Figure 5. Transmission electron microscopy images of MIT-1 (a,b), with selected-area diffraction patterns perpendicular to the plane of sheets (inset). Scanning electron microscopy images of MIT-1 (c,d).

Future work

To further reduce the costs associated with the process for producing MIT-1, we plan to focus on recycling the OSDA and reducing synthesis time and temperature. Molecular dynamics simulations with Ada-4-16 indicate that the structure-directing head sits inside of the cups of the MWW zeolite nanosheet with the diquaternary ammonium moieties stabilizing the pore mouth. This presents the possibility to recover the OSDA from the as-synthesized material for reuse in additional syntheses. In addition, removing the OSDA through extraction may allow us to reduce calcination temperatures to limit the formation of extraframework aluminum in the final product (see below).

Aim 2b: Characterize the distribution and activity of acid sites in MWW zeolite nanosheets for the activation of bulky substrates

Motivation and Objectives

Zeolites are highly active and selective heterogeneous catalysts used in many important chemical processes. The microporous crystalline frameworks of most aluminosilicates have high hydrothermal stability and feature attractive shape and transition-state selectivity effects. However, in some cases, microporosity hinders the diffusion of bulky molecules, resulting in lowered catalyst activity and faster deactivation. In our previous work, we found that hierarchical, MFI topology zeolite nanosheets (Al-MFI-ns) were very effective catalysts for the ring-opening hydrolysis of furfuryl alcohol to levulinic acid.[38] The nanosheet morphology of Al-MFI-ns provides larger surface areas and shorter molecular-diffusion lengths as compared to those of micron-sized zeolite crystals, while maintaining a crystalline structure associated with strong acid sites. Al-MFI-ns also demonstrated improved hydrothermal stability as compared to that of amorphous mesostructured silicates,

and slower deactivation from carbon deposition due to a larger number of external pore openings. Here we probe the nature of the acid sites found in MWW zeolite nanosheets, and test their activity for the Friedel-Crafts alkylation of bulky substrates.

Approach

The Brønsted acid sites in MIT-1 were probed with ^{27}Al MAS NMR as well as ^{31}P MAS NMR couple with adsorption of the phosphorus containing probe molecules. NMR measures the electron shielding around a targeted nucleus, which can be used as a highly sensitive method to study changes that arise from the effects in local electron density and overall electronegativity induced by neighboring atoms. ^{27}Al MAS NMR allows for the direct detection of the coordination environment of framework and extraframework aluminum sites. ^{31}P MAS NMR coupled with trialkylphosphine oxide probe molecules will allow us to assess the strength and distribution of the acid sites. Probe molecules trimethylphosphine oxide (TMPO) and tributylphosphine oxide (TBPO) interact strongly with both Brønsted and Lewis acid sites and do not require enrichment since the ^{31}P isotope is 100% natural abundance. The density of the electron cloud decreases with increasing acid strength, causing the ^{31}P resonance to shift toward a higher chemical shift compared to physisorbed TMPO (42 ppm). We performed vapor phase adsorption of TMPO and TBPO onto full dehydrated MIT-1 and benchmark MWW zeolites. Care was taken to ensure samples are kept under an inert environment and thermal annealing procedures (>423 K, 3 h) are performed to allow diffusion of TMPO molecules to all accessible active sites. The total acid sites of each type can be calculated by determining the P content in each material using elemental analysis with ICP-MS. The catalytic activity of externally accessible acid sites was probed with the liquid phase Friedel-Crafts alkylation of benzene with benzyl alcohol.

Results

The coordination environment of Al atoms was analyzed by ^{27}Al MAS NMR (see Figure 4B). MIT-1 with a Si/Al_{total} = 16.2 (as quantified from elemental analysis) features mainly tetrahedrally-coordinated framework Al species at 55 ppm with only a small fraction (<8%) of octahedrally coordinated extra-framework Al species present at 0 ppm. Note that the amount of extra-framework Al increases to *ca.* 30% after calcination, in agreement with previous reports by Corma *et al.* for MCM-22. [18] Calcination conditions require further optimization to minimize dealumination.

The number of internal and external acid sites were investigated with ^{31}P MAS NMR using trimethylphosphine oxide (TMPO) and tributylphosphine oxide (TBPO), respectively, as probe molecules. MCM-22, MCM-56, and MIT-1 have comparable peak signals at 85, 72, 68, and 63 ppm (Figure 6), which correspond to acid sites present in the 12-ring cages and 10-ring channels of MCM-22.[39] These chemical shifts are associated with strong Brønsted acid sites as determined by theoretical calculations between proton affinities and ^{31}P chemical shifts.[39] Additional peaks at 53, 42, and 31 ppm correspond to TMPO adsorbed onto Lewis acidic extra-framework Al, physisorbed TMPO, and crystalline TMPO, respectively. The total number of acid sites were quantified using spectra integration coupled with elemental analysis, showing 46, 32, and 33 x 10^{-5} mol g^{-1} for MCM-22, MCM-56, and

MIT-1, respectively (see Table 2). Following the same procedure, the external acid sites were probed with TBPO (*ca.* 0.8 nm), which cannot fit inside 10-ring channels. [40] MIT-1 had 21 x 10^{-5} mol g^{-1} of external acid sites, which is approximately three times more surface sites than those of MCM-22 (6 x 10^{-5} mol g^{-1}) and two time more surface sites than those of MCM-56 (13 x 10^{-5} mol g^{-1}). These values correspond well with the three and two-fold increases in external surface area for MIT-1 compared to MCM-22 and MCM-56.

The Friedel-Crafts alkylation of benzyl alcohol (BA) with benzene was used as a model reaction to assess the catalytic activity of MIT-1. Both the C-alkylation (diphenylmethane (DP)) and O- alkylation (dibenzyl ether (DE)) products are unable to fit inside 10-ring pores, thus limiting catalytic activity to the external surface for regular 3D zeolites. As shown in Table 3, MIT-1 converts 49% of BA after 1.5 h at 358 K with a DP yield of 23%. Nearly full conversion is observed after 3 h reaction time with a 65% yield of DP. After 5 h, the yield of DP increases to 99% as DE is reversibly converted back to BA, which is C-alkylated into DP. In contrast, MCM-22 and MCM-56 only reach 40% and 44% conversion after 3 h, respectively, at comparable Al loadings. Thus, Al-normalized rates at similar conversion levels show that MIT-1 has a three-fold increase in activity. This reactivity profile is proportional to the increase in external surface area and external acid site concentration of MIT-1 compared to MCM-22. Bulk Al-MFI zeolites showed negligible activity due to their low external surface areas. Al-MCM-41 also showed low activity for this reaction in agreement with Na *et al.* who showed that strong Brønsted acid sites are required to catalyze this reaction.[41]

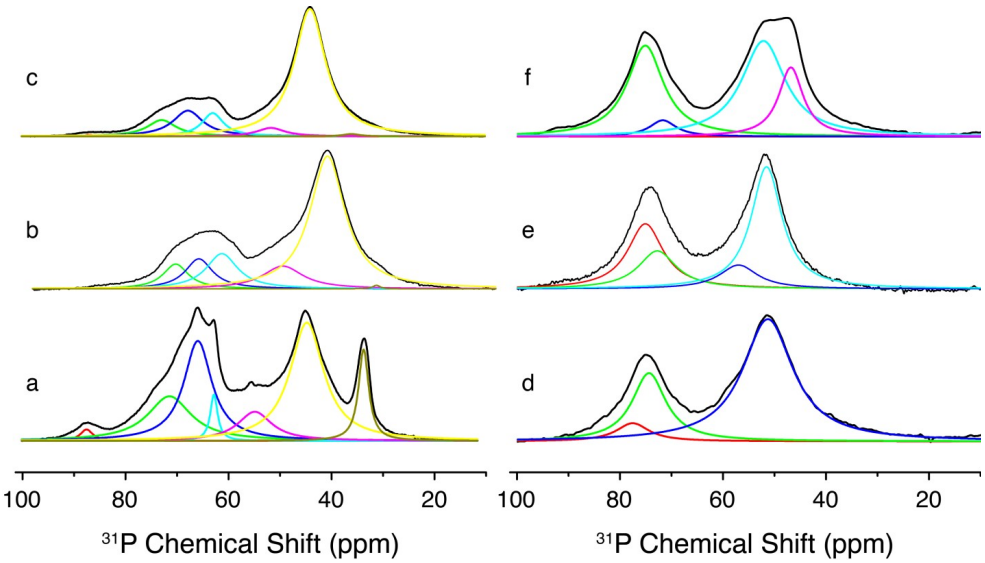

Figure 6. ^{31}P MAS NMR spectra of TMPO adsorbed onto MCM-22 (a), MCM-56 (b), MIT-1 (c); and TBPO adsorbed onto MCM-22 (d), MCM-56 (e), MIT-1 (f). A Lorentzian method was used for peak deconvolution.

Table 2. Properties of MCM-22, MCM-56, and MIT-1 zeolites.

Catalyst	Si/Al[a]	Micropore	Total pore volume[c]	S_{ext}[d] (m^2g^{-1})	Total acid sites[e] (x	External acid sites[f] (x 10^{-5}

		volume[b] (cm^3g^{-1})	(cm^3g^{-1})		10^{-5} mol g^{-1})	mol g^{-1})
MCM-22	25	0.142	0.289	121	46	6
MCM-56	12	0.133	0.601	219	32	13
MIT-1	16	0.131	1.014	513	33	21

a. Si/Al determined by ICP-AES elemental analysis, b. micropore volume calculated from N_2 adsorption isotherm at P/P_0=0.01, c. total pore volume calculated from N_2 adsorption isotherm at P/P_0=0.95, d. external surface area S_{ext} calculated using the t-plot method, e. total acid sites calculated from TMPO titration and ^{31}P MAS NMR, f. external acid sites calculated from TBPO titration and ^{31}P MAS NMR.

Table 3. Reactivity and selectivity data for the Friedel-Crafts alkyation of benzene with benzyl alcohol.

Catalyst	Conversion (%)	Yield DP (%)	Yield DE (%)
MCM-22	40	19	18
MCM-56	44	19	20
MIT-1	98	65	26
MIT-1[a]	49	23	21
MIT-1[b]	100	99	<1
Al-MCM-41	2	<1	<1
Al-MFI	3	<1	2

Reaction conditions: BA/Al = 200 mol/mol, 6.5 wt% BA in benzene, 3 h, 358 K. a. 1.5 h b. BA/Al = 100, 5 h, all other conditions the same.

Future work

Our next steps will focus on comparing the distribution of acid sites and catalytic activity of MIT-1 with other nanosheet morphology zeolites such as Al-MFI-ns. The local geometry of the pore environment around the tetrahedral Al active sites may dramatically affect the catalytic performance depending on the reactants and solvents. We will also further test MIT-1 for processes important for biomass conversion, and assess their stability in these processes.

Summary of main findings in this project:

1) Kinetics of transfer hydrogenation in Lewis-Brønsted acid pair catalysis: Performing rigorous kinetic studies is essential to compare the behavior of different Lewis acid catalysts. We conducted a comprehensive kinetic study on the liquid-phase MPV reduction of methyl levulinate to γ-valerolactone (GVL) over M-Beta zeolites. Experiments were carried out using flow reactors operating under differential conditions in the absence of mass transfer limitations. A rate expression was derived from a proposed set of elementary steps, and kinetic isotope effect studies were used to identify the rate-limiting step. We showed that, despite having significantly different initial TOFs, the apparent activation energies for Zr-, Hf-, and Sn-Beta were all approximately the same at ca. 52 kJ/mol and 73 kJ/mol for secondary and primary alcohol hydrogen donors, respectively. The difference in

activity, particularly when primary alcohol donors were used, was attributed to strong entropic effects (rather than to differences in the number of actives sites) expressed in the vastly different apparent pre-exponential factors with the order of Sn < Zr < Hf. These results suggest that in addition to intrinsic Lewis acid strength, geometric configurations within the pores also play an important role in determining catalytic activity. Extracting accurate kinetic parameters allowed us to effectively couple transfer hydrogenation sequences with hydrolytic ring-opening sequences for the one-pot conversion of furfural to GVL.

2) Development of hyperpolarization NMR techniques to confirm framework incorporation. The catalytic activity of Lewis acid zeolites for C-C coupling is critically dependent on the successful incorporation of the metal center into the zeolite framework. However, synchrotron-based techniques or MAS NMR of samples with "NMR-active" nuclei are the only reliable methods to verify framework incorporation. For ^{119}Sn-Beta (I=1/2, N.A.=8.6%), the coupled effects of low natural abundance of the ^{119}Sn isotope, low intrinsic NMR sensitivity (based on Sn's low gyromagnetic ratio), and low Sn loadings in the zeolite (<3 wt%) make MAS NMR analysis impractical without ^{119}Sn isotope enrichment. Unfortunately, the high cost of isotopic enrichment drastically hinders high-throughput screening, routine analysis, or analysis of low-yield syntheses with NMR. This analysis is even more difficult for highly quadrupolar nuclei, such as Ti and Zr.

DNP tackles the challenge of increasing spin polarization by transferring the larger polarization of electron spins, such as those found in stable radical compounds, to nuclear spins through irradiation with high-frequency microwaves. The nuclei of the target species then become dynamically polarized, and their NMR signals are enhanced by up to four orders of magnitude. Additional signal enhancements can be obtained by doing experiments at temperatures down to 1 K. We demonstrated for the first time, the use of DNP NMR for characterizing zeolites containing ~ 2 wt % of natural abundance Sn without the need for ^{119}Sn isotopic enrichment. The biradicals TOTAPOL, bTbK, bCTbK, and SPIROPOL functioned effectively as polarizing sources, and the solvent enabled proper transfer of spin polarization from the radical' s unpaired electrons to the target nuclei. Using bCTbK led to an enhancement of 75, allowing the characterization of natural-abundance ^{119}Sn-Beta with excellent signal-to-noise ratios in <24 h. Without DNP, no ^{119}Sn resonances were detected after 10 days of continuous analysis. Given that DNP reduces the collection time of NMR data by orders of magnitude, it allows to fully exploit the realm of information provided by more advanced NMR experiments typically restricted to liquid-phase analysis (e.g., two-dimensional spectra of unlabeled molecules).

3) Triggering C-C coupling with acid-base pairs in Lewis acid zeolites. Natural and synthetic systems exploit the cooperative interactions among acid-base pairs to promote C-C bond formation reactions. For example, class II aldolases catalyze the direct aldol reaction of dihydroxyacetone phosphate (DHAP) and aldehydes through a cooperative activation called soft enolization. The proposed transition-state model for the active sites of this lyase shows that the Lewis acid site Zn^{II} coordinates to the carbonyl oxygen of the ketone donor, while a glutamate residue functions as a Brønsted base for abstraction of the α-proton and subsequent enol formation. In Lewis acid zeolites, soft enolization results in the formation of a Sn-enolate intermediate and the cleavage of one Si−O−Sn bond. We investigated the keto–enol

tautomerization mechanism using deuterated acetone with NMR and provided the first mechanistic proof that the acid-base pairs in Sn- and Hf-Beta promote C-D activation followed by the intramolecular transfer of an α-deuterium atom to the zeolite lattice. UV/Vis and ^{119}Sn NMR analyses ruled out the presence of high concentrations of extraframework tin oxide species, corroborating that keto-enol tautomerization is mainly catalyzed by the framework metal active centers. Our group then demonstrated the application of Sn-Beta for the catalytic C–C coupling between DHA and formaldehyde to form the synthetically useful compound α-hydroxy-γ-butyrolactone (HBL). We showed that Sn-, Hf- and Zr-Beta generated near quantitative yields of the single cross-aldol condensation product from the coupling of substituted aromatic aldehydes with acetone. Notably, unlike regular heterogeneous base catalysts used in aldol condensations (e.g., MgO), our materials maintained activity and showed exceptional stability **in the presence of considerable amounts of water and acetic acid contaminants**.

C) Special recognitions received by PI

NSF CAREER Award

D) Statement of unspent funds for the year

To date, 100% of the original funds have been spent.

E) List of pending and current support

Status of Funding: Current
Source of Support: Masdar Institute of Science and Technology
Title of Award: BIOREFINERY – Integrated Sustainable Process for Biomass Conversion to Biomaterial, Biofuels and Fertilizer
Award Period: 07/01/2013 – 06/30/2016
Total Award Amount for Award Period: $423,011
Number of person-months/ yr. supported: 0.5 summer months

Status of Funding: Current
Source of Support: BP Technology Ventures, Inc.
Title of Award: Catalytic Upgrading Fab Equipment
Award Period: 03/01/2012 – 08/31/2016
Total Award Amount for Award Period: $18,000
Number of person-months/ yr. supported: 1 summer months

Status of Funding: Current
Source of Support: BP Technology Ventures, Inc.
Title of Award: Catalytic Upgrading of Pyrolysis Streams
Award Period: 03/01/2012 – 08/31/2016
Total Award Amount for Award Period: $2,183,042
Number of person-months/ yr. supported: 0.75 summer months

Status of Funding: Current
Source of Support: BP Technology Ventures, Inc.
Title of Award: Fabricated Equipment – Flow Reactor Platform for Testing Bio-Oils
Award Period: 09/01/2012 – 08/31/2016
Total Award Amount for Award Period: $8,179
Number of person-months/ yr. supported: 0 summer months

Status of Funding: Current
Source of Support: ARAMCO Services Company
Title of Award: Industrial Heterogeneous Catalysts for Olefin Metathesis
Award Period: 10/01/2014 – 09/30/2019
Total Award Amount for Award Period: $744,777
Number of person-months/ yr. supported: 0.5 calendar months

Status of Funding: Current
Source of Support: ARAMCO Services Company
Title of Award: Fabricated Equipment – Flow Reactor Platform
Award Period: 09/01/2015 – 09/30/2016
Total Award Amount for Award Period: $38,343
Number of person-months/ yr. supported: 0 calendar months

Status of Funding: Current
Source of Support: NSF
Title of Award: Molecular Catalysis for Waste Valorization
Award Period: 01/01/2015 – 12/31/2019
Total Award Amount for Award Period: $500,001
Number of person-months/ yr. supported: 0.25 summer months

Status of Funding: Pending
Source of Support: NSF
Title of Award: Unifying Hydrodeoxygenation Mechanisms of Bio-Derived Feedstock over Early Transition Metal Oxides and Carbides
Award Period: 06/01/2016 – 05/31/2019
Total Award Amount for Award Period: $645,686
Number of person-months/ yr. supported: 0.50 summer month

Status of Funding: Pending
Source of Support: NSF
Title of Award: Zeolite Nanosheets as a Multi-Functional Catalytic Platform for Biomass Conversion
Award Period: 06/01/2016 – 05/31/2019
Total Award Amount for Award Period: $299,981
Number of person-months/ yr. supported: 0.25 summer month

Status of Funding: Pending
Source of Support: DOE - EERE
Title of Award: Tandem Lignin Deconstruction and Valorization via Coupled Chemo – and Bio-Catalysis
Award Period: 03/01/2016 – 02/28/2018
Total Award Amount for Award Period: $1,354,000
Number of person-months/ yr. supported: 1 summer month

Status of Funding: Pending
Source of Support: DOE
Title of Award: Molecular Understanding of Bifunctional Solid Lewis Acid Zeolites for the C-C Coupling of Alpha Keto Acids
Award Period: 06/01/2016 – 05/31/2019
Total Award Amount for Award Period: $449,998
Number of person-months/ yr. supported: 0.25 summer month/year 1

Status of Funding: Pending

Source of Support: NSF
Title of Award: DMREF: First-Principles Design of Metal-Organic Framework Catalysts for Selective Epoxidation
Award Period: 08/01/2016 – 07/31/2020
Total Award Amount for Award Period: $1,500,000
Number of person-months/ yr. supported: 0.25 summer month/year 1

Status of Funding: Pending
Source of Support: NSF
Title of Award: INFEWS/T3: Guided Catalyst Design for Endocrine Disruptor Removal from Wastewater Streams
Award Period: 10/01/2016 – 09/30/2019
Total Award Amount for Award Period: $1,000,000
Number of person-months/ yr. supported: 0.50 summer month/year

Please note: *Levels of summer effort will be adjusted if multiple projects are awarded*

F) Complete list of publications:

Sole funding by DOE-BES and this grant

Funding by this grant:

1. Luo, H., Lewis, J. D., & Román-Leshkov, Y.* Lewis Acid Zeolites for Biomass Conversion: Perspectives and Challenges on Reactivity, Synthesis, and Stability. Annu. Rev. Chem. Biomol. Eng. 7 (2016).
2. Wang, Y., Lewis, J. D., & Román-Leshkov, Y.* Synthesis of Itaconic Acid Ester Analogues via Self-Aldol Condensation of Ethyl Pyruvate Catalyzed by Hafnium BEA Zeolites. ACS Catal. ASAP doi:10.1021/acscatal.6b00561 (2016).
3. Van de Vyver, S. & Román-Leshkov, Y.* Metalloenzyme-Like Zeolites as Lewis Acid Catalysts for C-C Bond Formation. Angew. Chem. Int. Ed. 54:12554-12561 (2015).
4. Luo, H. Y., Michaelis, V. K., Hodges, S. Griffin, R. G., & Román-Leshkov, Y.* One-pot synthesis of MWW zeolite nanosheets using a rationally designed organic structure-directing agent. Chem. Sci. 6:6320-6324 (2015).
5. Lewis, J. D., van de Vyver, S., & Román-Leshkov, Y.* Acid-Base Pairs in Lewis-Acidic Zeolites Promote Direct Aldol Reactions by Soft Enolization. Angew. Chem. Int. Ed. 54:9835-9838 (2015).
6. Luo, H. Y. & Román-Leshkov, Y.* Al-MFI Nanosheets as highly active and stable catalysts for the conversion of propanal to hydrocarbons. Top. Catal., 58:529-536 (2015).
7. Hunt, S., Kokumai, T., Zanchet, D., & Román-Leshkov, Y.* Bimetallic Tantalum Tungsten Carbide Nanoparticles Exhibit High Hydrogen Evolution Activity and Increased Electrochemical Oxidation Resistance. J. Phys. Chem. C., 119:3691-13699 (2015).
8. Van de Vyver, S., Odermatt, C., Romero, K., & Román-Leshkov, Y.* Solid Lewis Acids Catalyze the Carbon−Carbon Coupling of Biomass-Derived Molecules with Formaldehyde. ACS. Catal. 5:972–977 (2015).

9. Luo, H., Consoli, D., Gunther, W. R., & Román-Leshkov, Y.* Investigation of the reaction kinetics of isolated Lewis acid sites in Beta zeolites for the Meerwein-Ponndorf-Verley reduction of methyl levulinate to γ-valerolactone. J. Catal. 320:198–207(2014).
10. Lewis, J. D., Van de Vyver, S., Crisci, A. J., Gunther, W. R., Michaelis, V. K., Griffin, R. G., & Román-Leshkov, Y.* A Continuous Flow Strategy for the Coupled Transfer Hydrogenation and Etherification of 5-(Hydroxymethyl)furfural using Lewis Acid Zeolites. ChemSusChem 7:2255–2265 (2014).
11. Gunther, W.R., Michaelis, V. K., Caporini, M. A., Griffin, R. G., & Román-Leshkov, Y.* Dynamic nuclear polarization NMR enables the analysis of Sn-Beta zeolite prepared with natural abundance ^{119}Sn precursors. J. Am. Chem. Soc. 136:6219-6222 (2014).
12. Hunt, S. T., Nimmanwudipong, T. & Román-Leshkov, Y.* Engineering Non-sintered, Metal-terminated Tungsten Carbide Nanoparticles for Catalysis. Angew. Chem. Int. Ed. 53:5131-5136 (2014).
13. Gunther, W. R., Duong, Q., & Román-Leshkov, Y.* Catalytic consequences of borate complexation and pH on the epimerization of L-arabinose to L-ribose in water catalyzed by Sn-Beta zeolite with borate salts. J. Mol. Catal. A: Chem. 379:294-302 (2013).
14. Bui, L., Luo, H., Gunther, W. R. & Román-Leshkov, Y.* Domino reaction for the production of gamma-valerolactone from furfural catalyzed by zeolites with Brønsted and Lewis acid sites. Angew. Chem. Int. Ed. 52:8022-8025 (2013). (Hot Article and Inside Cover)

Funding from DOE-BES:

1. Bermejo-Deval, R., Assary, R.S, Nikolla, E., Moliner, M., Román-Leshkov, Y., Huang, SJ., Palsdottir, A., Silverman, D., Lobo, R.F., Curtiss, L., & Davis, M.E. Metalloenzyme-like catalyzed isomerizations of sugars by Lewis acid zeolites. **Proc. Nat. Acad. Sci.** 109, 9727-9732 (2012).
2. Nikolla, E., Román-Leshkov, Y., Moliner, M. & Davis, M. E. “One-Pot” Synthesis of 5-(Hydroxymethyl)furfural from Carbohydrates using Tin-Beta Zeolite. **ACS Catal.** 1, 408-410 (2011).
3. Román-Leshkov, Y., Moliner M., Labinger J. & Davis, M.E. Mechanism of Glucose Isomerization Using a Solid Lewis Acid Catalyst in Water. **Angew. Chem. Int. Ed**. 49, 8954-8957 (2010).
4. Moliner M., Román-Leshkov, Y., & Davis, M.E. Tin-containing Zeolites are Highly Active Catalysts for the Isomerization of Glucose in Water. **Proc. Natl. Acad. Sci**. **U.S.** 107, 6164-6168 (2010).

Joint funding by DOE and other sources

1. Chen, H. S., Wang, A., Sorek, H., Lewis, J. D., Román-Leshkov, Y., & Bell, A. T.* Production of Hydroxyl-rich Acids from Xylose and Glucose Using Sn-BEA Zeolite Submitted (2015).

2. Kumar, M., Luo, H., Román-Leshkov, Y., & Rimer, J. D.* SSZ-13 crystallization by particle attachment and deterministic pathways to crystal size control. J. Am. Chem. Soc. 137:13007-13017 (2015).
3. Abdelrahman, O. A., Luo, H. Y., Heyden, A., Román-Leshkov, Y. & Bond, J. Towards rational design of stable, supported metal catalysts for aqueous phase processing: insights from the hydrogenation of levulinic acid.J. Catal. 329:10–21 (2015).

Sole funding by other sources

1. Said, S. A., Simakov, D. S., Waseeuddin, M., & Román-Leshkov, Y.* Solar membrane reformer heated with molten salt for natural gas upgrading and hydrogen generation: a CFD model. Solar Ener. 124:163-176 (2016).
2. Shetty, M., Murugappan, K., Prasomsri, T., Green, W. H., & Román-Leshkov, Y.* Reactivity and stability investigation of supported molybdenum oxide catalysts for the hydrodeoxygenation (HDO) of m-cresol. J. Catal. 331:86-97 (2015).
3. Wright, M., Seifkar, N., Green, W. H., & Román-Leshkov, Y.* Natural Gas and Cellulosic Biomass: a Clean Fuel Combination? Determining the Natural Gas Blending Wall in Biofuel Production. Environ. Sci. Technol. 49:8183-8192 (2015).
4. Wang, Y., Vogelgsang, F., & Román-Leshkov, Y.* Acid-catalyzed oxidation of levulinate derivatives to succinates under mild conditions. ChemCatChem 7:916-920 (2015).
5. Said, S. A., Simakov, D. S., Mokheimer, E. M., Habib, M. A., Ahmed, S., Waseeuddin, M., & Román-Leshkov, Y.* Computational fluid dynamics study of hydrogen generation by low temperature methane reforming in a membrane reactor. Int. J. Hydrogen Energy 40:3158–3169 (2015).
6. Narsimhan, K., Michaelis, V. K., Mathies, G., Gunther, W. R., Griffin, R. G., & Román-Leshkov, Y.* Production of Acetic Acid from Methane via Tandem Oxidation and Carbonylation on Copper Exchanged Mordenite Zeolites. J. Am. Chem. Soc. 137:1825–1832 (2015).
7. Simakov, D. S., Wright, M., Ahmed, S., Mokheimer, E. M., & Román-Leshkov, Y.* Solar thermal catalytic reforming of natural gas: a review on chemistry, catalysis and system design. Catal. Sci. Technol. 5:1991-2006 (2015).
8. Crisci, A. J., Dou, H., Prasomsri, T., & Román-Leshkov, Y. Cascade Reactions for the Continuous and Selective Production of Isobutene from Bio-derived Acetic Acid Over Zinc-Zirconia Catalysts. ACS. Catal. 4:4196-4200 (2014).
9. Bruijnincx, P. C. A.* & Román-Leshkov, Y.* Sustainable catalytic conversions of renewable substrates. Catal. Sci. Technol. 4:2180-2181 (2014).
10. Prasomsri, T., Shetty, M., Murugappan, K., & Román-Leshkov, Y.* Insights into the catalytic activity and surface modification of MoO3 during the hydrodeoxygenation of lignin-derived compounds into aromatic hydrocarbons under mild conditions. Energy Environ. Sci. 7:2660-2669 (2014). (Selected for back cover)
11. Wang, Y., Van de Vyver, S., Sharma, K. K., & Román-Leshkov, Y.* Insights into the stability of gold nanoparticles supported on metal oxides for the base-free oxidation of glucose to gluconic acid. Green Chem. 6:719-726 (2014).
12. Prasomsri, T., Nimmanwudipong, T. & Román-Leshkov, Y. Effective hydrodeoxygenation of biomass-derived oxygenates into unsaturated

hydrocarbons by MoO3 using low H2 pressures. **Energy Environ. Sci**. 6:1732-1738 (2013). (Inside Cover)
13. Van de Vyver, S. &, Román-Leshkov, Y. Emerging catalytic processes for the production of adipic acid. **Catal. Sci. Technol.**, 3:1465-1479 (2013).
14. Van de Vyver, S., Helsen,S., Geboers, J., Yu,F., Thomas, J., Smet, M., Dehaen,W, Román-Leshkov, Y., Hermans, I., & Sels, B.F. Mechanistic Insights into the Kinetic and Regiochemical Control of the Thiol-Promoted Catalytic Synthesis of Diphenolic Acid. **ACS Catal**. 2, 2700-2704 (2012).
15. Luo, H. Y., Bui, L., Gunther, W.R., Min, E. & Román-Leshkov, Y. Synthesis and catalytic activity of Sn-MFI Nanosheets for the Baeyer-Villiger oxidation of cyclic ketones. **ACS Catal**., 2, 2695-2699 (2012).
16. Gunther, W.R., Wang, Y., Ji, Y., Michaelis, V.K., Hunt, S.T., Griffin, R.G., & Román-Leshkov, Y. Sn-Beta zeolites with borate salts catalyse the epimerization of carbohydrates via an intramolecular carbon shift. **Nat. Comm.**, 3, 1109-1115 (2012).
17. Wright, M.M., Román-Leshkov, Y. & Green, W.H. Investigating the techno-economic tradeoffs of hydrogen source using a response surface model of drop-in biofuel production via bio-oil upgrading. **Biofuels, Bioprod. Biorefin.**6, 503-520 (2012).
18. Zahmakıran, M., Román-Leshkov, Y. & Zhang, Y. Rhodium(0) Nanoparticles Supported on Nanocrystalline Hydroxyapatite: Highly Effective Catalytic System for the Solvent-Free Hydrogenation of Aromatics at Room Temperature. **Langmuir** 28, 60–64 (2012).
19. Román-Leshkov, Y. & Davis, M. E. Activation of Carbonyl-Containing Molecules with Solid Lewis Acids in Aqueous Media. **ACS Catal.** 1, 1566–1580 (2011).
20. Román-Leshkov, Y., Moliner M. & Davis, M.E. Impact of controlling the site distribution of Al atoms on catalytic properties in ferrierite-type zeolites. **J. Phys. Chem. C** 115, 1096-1102 (2011).
21. Román-Leshkov, Y., Moliner M. & Davis, M.E. Hybrid, organic-inorganic solids that show shape selectivity. **Chem. Mat.** *22*, 2646 (2010).
22. Román-Leshkov, Y. & Dumesic, J. A. Solvent Effects on Fructose Dehydration to 5-Hydroxymethylfurfural in Biphasic Systems Saturated with Inorganic Salts. **Top. Catal.** 52, 297-303 (2009).
23. Román-Leshkov, Y., Barrett, C. J., Liu, Z. Y. & Dumesic, J. A. Production of dimethylfuran for liquid fuels from biomass-derived carbohydrates. **Nature** 447, 982-985 (2007).
24. Chheda, J. N., Román-Leshkov, Y. & Dumesic, J. A. Production of 5-hydroxymethylfurfural and furfural by dehydration of biomass-derived mono-and poly-saccharides. **Green Chem.** 9, 342-350 (2007).
25. Román-Leshkov, Y., Chheda, J. N. & Dumesic, J. A. Phase modifiers promote efficient production of hydroxymethylfurfural from fructose. **Science** 312, 1933-1937 (2006).

References for the results section

[1] J. Lauwaert, E.G. Moschetta, P. Van Der Voort, J.W. Thybaut, C.W. Jones, G.B. Marin, J. Catal., 325 (2015) 19-25.
[2] T.D. Machajewski, C.-H. Wong, Angew. Chem. Int. Ed., 39 (2000) 1352-1375.
[3] N. Kumagai, M. Shibasaki, Angew. Chem. Int. Ed., 50 (2011) 4760-4772.

[4] M.S. Holm, Y.J. Pagan-Torres, S. Saravanamurugan, A. Riisager, J.A. Dumesic, E. Taarning, Green Chem., 14 (2012) 702-706.
[5] J. Dijkmans, M. Dusselier, D. Gabriëls, K. Houthoofd, P.C.M.M. Magusin, S. Huang, Y. Pontikes, M. Trekels, A. Vantomme, L. Giebeler, S. Oswald, B.F. Sels, ACS Catal., 5 (2015) 928-940.
[6] S. Van de Vyver, C. Odermatt, K. Romero, T. Prasomsri, Y. Román-Leshkov, ACS Catal., (2015) 972-977.
[7] Y.-P. Li, M. Head-Gordon, A.T. Bell, ACS Catal., 4 (2014) 1537-1545.
[8] R. Bermejo-Deval, R. Gounder, M.E. Davis, ACS Catal., 2 (2012) 2705-2713.
[9] G.W. Huber, J.N. Chheda, C.J. Barrett, J.A. Dumesic, Science, 308 (2005) 1446-1450.
[10] L. Hora, V. Kelbichová, O. Kikhtyanin, O. Bortnovskiy, D. Kubička, Catal. Today, 223 (2014) 138-147.
[11] R.M. West, Z.Y. Liu, M. Peter, C.A. Gärtner, J.A. Dumesic, J. Mol. Catal. A: Chem., 296 (2008) 18-27.
[12] M. Boronat, A. Corma, M. Renz, J Phys Chem B, 110 (2006) 21168-21174.
[13] J.D. Lewis, S. Van de Vyver, A.J. Crisci, W.R. Gunther, V.K. Michaelis, R.G. Griffin, Y. Román-Leshkov, ChemSusChem, 7 (2014) 2255-2265.
[14] M.K. Rubin, P. Chu, Composition of synthetic porous crystalline material, its synthesis and use, in, Google Patents, 1990.
[15] M.E. Leonowicz, J.A. Lawton, S.L. Lawton, M.K. Rubin, Science, 264 (1994) 1910-1913.
[16] S. Lawton, M. Leonowicz, R. Partridge, P. Chu, M. Rubin, Microporous and Mesoporous Materials, 23 (1998) 109-117.
[17] A. Corma, V. Martınez-Soria, E. Schnoeveld, Journal of catalysis, 192 (2000) 163-173.
[18] A. Corma, C. Corell, V. Fornés, W. Kolodziejski, J. Pérez-Pariente, Zeolites, 15 (1995) 576-582.
[19] A. Corma, V. Fornes, S. Pergher, T.L. Maesen, J. Buglass, Nature, 396 (1998) 353-356.
[20] A. Corma, V. Gonzalez-Alfaro, A. Orchillés, Journal of Catalysis, 200 (2001) 34-44.
[21] A. Corma, V. Fornés, J. Guil, S. Pergher, T.L. Maesen, J. Buglass, Microporous and mesoporous materials, 38 (2000) 301-309.
[22] R. Schenkel, J.-O. Barth, J. Kornatowski, J. Lercher, Studies in Surface Science and Catalysis, 142 (2002) 69-76.
[23] A.S. Fung, S.L. Lawton, W.J. Roth, Synthetic layered MCM-56, its synthesis and use, in, Google Patents, 1994.
[24] G.G. Juttu, R.F. Lobo, Microporous and mesoporous materials, 40 (2000) 9-23.
[25] A. Corma, U. Diaz, V. Fornés, J. Guil, J. Martinez-Triguero, E. Creyghton, Journal of Catalysis, 191 (2000) 218-224.
[26] A. Corma, M.J. Díaz-Cabanas, M. Moliner, C. Martínez, Journal of Catalysis, 241 (2006) 312-318.
[27] W.J. Roth, D.L. Dorset, G.J. Kennedy, Microporous and Mesoporous Materials, 142 (2011) 168-177.
[28] M.A. Camblor, L.A. Villaescusa, M. Diaz-Cabanas, Topics in Catalysis, 9 (1999) 59-76.
[29] R.F. Lobo, S.I. Zones, M.E. Davis, Journal of inclusion phenomena and molecular recognition in chemistry, 21 (1995) 47-78.

[30] W. Park, D. Yu, K. Na, K.E. Jelfs, B. Slater, Y. Sakamoto, R. Ryoo, Chemistry of Materials, 23 (2011) 5131-5137.
[31] P. Chu, Zeolite zsm-48, in, Google Patents, 1983.
[32] J. Schlenker, W. Rohrbaugh, P. Chu, E. Valyocsik, G. Kokotailo, Zeolites, 5 (1985) 355-358.
[33] R.F. Lobo, H. van Koningsveld, Journal of the American Chemical Society, 124 (2002) 13222-13230.
[34] U. Díaz, ISRN Chemical Engineering, 2012 (2012).
[35] J. Schlenker, B. Peterson, Journal of applied crystallography, 29 (1996) 178-185.
[36] J. Boshoff, http://www.che.udel.edu/research_groups/nanomodeling/resources.html, University of Delaware (2012).
[37] I. Ogino, M.M. Nigra, S.-J. Hwang, J.-M. Ha, T. Rea, S.I. Zones, A. Katz, Journal of the American Chemical Society, 133 (2011) 3288-3291.
[38] L. Bui, H. Luo, W.R. Gunther, Y. Román-Leshkov, Angewandte Chemie International Edition, 52 (2013) 8022-8025.
[39] A. Zheng, L. Chen, J. Yang, M. Zhang, Y. Su, Y. Yue, C. Ye, F. Deng, The Journal of Physical Chemistry B, 109 (2005) 24273-24279.
[40] Y. Seo, K. Cho, Y. Jung, R. Ryoo, ACS Catalysis, 3 (2013) 713-720.
[41] K. Na, C. Jo, J. Kim, K. Cho, J. Jung, Y. Seo, R.J. Messinger, B.F. Chmelka, R. Ryoo, Science, 333 (2011) 328-332.